Modelling and Simulation in Materials Science and Engineering

Determination of thermal conductivity of eutectic Al–Cu compounds utilizing experiments, molecular dynamics simulations and machine learning

To cite this article: A Nazarahari *et al* 2023 *Modelling Simul. Mater. Sci. Eng.* **31** 045001

OPEN ACCESS
IOP Publishing
Modelling and Simulation in Materials Science and Engineering
Modelling Simul. Mater. Sci. Eng. **31** (2023) 045001 (18pp) https://doi.org/10.1088/1361-651X/acc960

Determination of thermal conductivity of eutectic Al–Cu compounds utilizing experiments, molecular dynamics simulations and machine learning

A Nazarahari[1], A C Fromm[2], H C Ozdemir[1], C Klose[2], H J Maier[2,*] and D Canadinc[1]

[1] Department of Mechanical Engineering, Koc University, Advanced Materials Group (AMG), Istanbul 34450, Turkey
[2] Leibniz Universität Hannover, Institut für Werkstoffkunde (Materials Science), An der Universität 2, 30823 Garbsen, Germany

E-mail: maier@iw.uni-hannover.de

Received 10 February 2023; revised 23 March 2023
Accepted for publication 31 March 2023
Published 14 April 2023

Abstract

In this study, the thermal conductivity (κ) of Al–Cu eutectics were investigated by experimental and computational methods to shed light on the role of these compounds in thermal properties of Al–Cu connections in compound casting. Specifically, the nonequilibrium molecular dynamics (MD) method was utilized to simulate the lattice thermal conductivity (κ_l) of six compositions of Al–Cu with 5–30 at.% Cu. To extend the results of the MD simulations to bulk materials, instead of using conventional linear extrapolation methods, a machine learning approach was developed for the dataset acquired from the MD simulations. The bootstrapping approach was utilized to find the most suitable method among the support vector machine (SVM) with polynomial and radial basis function (RBF) kernels and the random forest method. The results showed that the SVM model with RBF kernel performed the best, and thus was used to predict the bulk κ_l. Subsequently, the chosen compositions were produced by induction casting and their electrical conductivities were measured via eddy current method for calculating the electronic contribution of κ using the Wiedemann–Franz law. Finally, the actual κ of the alloys were

* Author to whom any correspondence should be addressed.

measured using the xenon flash method and the results were compared with the computational values. It was shown that the MD method is capable of successfully simulating the thermal conductivity of this system. In addition, the experimental results demonstrated that the κ of Al–Cu eutectics decreases almost linearly with formation of the Al_2Cu phase due to increase in the Cu content. Overall, the current findings can be used to enhance the κ of cooling devices made via Al–Cu compound casting.

Supplementary material for this article is available online

Keywords: thermal conductivity, molecular dynamics, machine learning, Al–Cu eutectics, Wiedemann–Franz law

(Some figures may appear in colour only in the online journal)

1. Introduction

Cooling efficiency is of utmost importance for the design of electronic components with superior performance [1]. One of the essential parameters affecting the cooling performance is the thermal conductivity (κ), and copper is the material of choice for this purpose due to its high κ; however, the high density of copper (8.96 g cm^{-3}) and material costs restrict its utility for monolithic components. As a result, cooling components are made by coupling copper with aluminum that has a lower density (2.7 g cm^{-3}) at the expense of lowering the overall κ. Previous studies showed that poor connection at the Al and Cu component surfaces is one of the main issues that decrease the overall cooling capability of the components [2]. Currently, various thermal interface materials (TIMs) such as polymer-based composites containing copper or alumina are used between the components in the form of pads, gels or adhesives to reduce contact resistance [1, 3, 4]. However, such materials have substantially lower κ than the bulk Al and Cu [5], and thus significantly decrease the efficiency of the cooling component. A solution to this problem is to replace the TIMs with compound casting of Al on Cu components. With this approach, the molten Al is cast on the copper component, forming a metallic bond, eliminating the need for TIMs, and lowering the contact resistance. Although this process is deemed simple, the natural oxides on the surface of the components suppress wetting and work as a barrier, resulting in a poor connection, and thereby leading to undesirable mechanical properties and limited thermal conductivity [2, 6].

In order to eliminate the adverse effect of natural oxides on parts manufactured by compound casting, a new approach has been proposed, where the casting process is performed under extremely high vacuum (XHV) adequate atmosphere using silane gas to remove the residual oxygen present in the environment [7–9]. Since the partial pressure of the oxygen is extremely low in such atmospheres, the formation of natural oxides on the cleaned surfaces of copper is inhibited, enhancing the metallic bond formation [7, 8]. As expected, during solidification and formation of such bonds, diffusion of atoms would create a compositional gradient at the connection interface. Previous studies showed that under XHV atmosphere, the interface, where Al–Cu connection takes place, is mainly composed of the Al-rich eutectic range of the Al–Cu phase diagram and the θ-phase (Al_2Cu), followed by thin layers of intermetallic compounds such as AlCu (η) and Al_4Cu_9 (γ) [8]. Considering that the compositional gradient of these layers could significantly affect the overall κ of the cooling component, it is crucial to optimize the casting parameters so that the relative fraction of each phase can be controlled

to obtain the best thermal conductivity. However, this goal is not achievable without a proper understanding of κ in this region.

The thermal conductivity of metals and alloys is made of two components $\kappa = \kappa_e + \kappa_l$, where κ_e is the electronic and the κ_l is the lattice contribution to κ. The component κ_e is commonly calculated via the Wiedemann–Franz law (WFL) equation that converts the electrical conductivity (σ) to κ_e:

$$\kappa_e = \sigma \times T \times L \tag{1}$$

where T is the absolute temperature, and L is a constant known as the Lorenz number.

The substantial contribution of electrons to κ is known for materials with high electrical conductivity, such as pure Cu, Al, and Au [10]. Therefore, the WFL is a common method to estimate the κ since the σ is readily available for many materials. Also, if σ is not available, its experimental measurement is simple and less complicated than the direct measurement of κ. Although some studies approved this estimation for some alloys and intermetallics, such as Sn–37 Pb, Cu_3Sn and Cu_6S_5 [11], several other studies showed that this equation does not hold for other alloy systems and intermetallic compounds. The shortcoming of the WFL method is a consequence of the change in the electrons' mean free path, which is affected by crystal defects and scattering of electrons. In addition, the higher contribution of κ_l in such materials is discarded by the WFL, which can result in some deviation from the actual value of κ [12, 13]. Therefore, it can be deduced that by complementing the κ_e calculated using the WFL by κ_l, the overall κ can be calculated with enhanced accuracy. However, the calculation of κ_l demands a good understanding of the thermal conduction through the crystal lattice.

The κ_l is generated from the transfer of vibrational energy of atoms by progressive waves, also known as phonons. These phonons propagate through materials and have a mean free path that is governed by interactions with the other phonons, free electrons, and defects [14]. Such scatterings, also known as Umklapp scatterings, are more pronounced in impure materials and it is necessary to consider them when calculating the κ_l [15]. Some studies have tried the calculation of the κ_l via analytical methods [16]; however, due to the complex behaviors of such scatterings, an accurate calculation of the κ_l is only possible through computational methods that consider the vibration of atoms.

One of the methods to calculate the κ_l is atomistic simulations, and for this purpose, one of the strongest candidates in terms of accuracy is density functional theory (DFT). However, the computational cost of employing DFT simulations in the solution of problems involving numerous compositions is significant. A more efficient solution for calculating κ_l is molecular dynamics (MD), where κ_l can be simulated via equilibrium or nonequilibrium approaches. In an equilibrium approach, heat flux is applied to the system, and the resulting thermal gradient until equilibration is used for calculating the κ_l. As an example, the Green–Kobo method uses an equilibrium approach that has proved to be successful in predicting κ_l of various materials [17, 18]. However, in some materials, this method has the disadvantage of slow convergence, as it is necessary to simulate periods several times longer than the longest phonon relaxation time to achieve accurate results [19]. Another approach is to use nonequilibrium methods such as the Müller-Plathe method, also known as reverse nonequilibrium molecular dynamics (NEMD). As opposed to the Green–Kobo method, this method applies the thermal gradient in the system and measures the resulting heat flux to calculate the κ_l. As a result, it provides several advantages, such as substantially lower computational cost, faster convergence, and better compatibility with periodic boundary conditions. It should be noted that the relative efficiency of the equilibrium and nonequilibrium methods are dependent on the properties of

the material, and since the Al–Cu system studied in this work is isotropic, the NEMD method can be a useful and efficient tool to simulate κ_l for this system [20, 21].

With this motivation, the Müller-Plathe method was employed to determine the κ_l of six Al–Cu compositions with 5, 10, 15, 20, 25, and 30 at.% Cu in the current study investigating the thermal conductivity of Al–Cu eutectic compounds. In order to adapt the computed values to bulk materials, a machine learning (ML) approach was utilized to predict the bulk κ_l as several recent studies suggest the use of ML to predict the thermal transport properties of materials with enhanced accuracy [22–24]. Subsequently, to validate the results, samples with the aforementioned compositions were cast utilizing vacuum induction melting, heat treated for recrystallization and growth, and their electrical conductivity was measured utilizing an eddy current method, such that it could be incorporated into the WFL equation to calculate their κ_e. Finally, their thermal conductivities were directly measured using the xenon flash method and were compared with the sum of κ_e and κ_l. The results suggested that the use of ML in conjunction with MD simulations for predicting κ_l for bulk materials is a promising method that can eliminate the problems associated with linear extrapolation. Moreover, the addition of κ_l to the values acquired from the WFL equation can enhance the accuracy of the calculated κ, providing a replacement for the direct measurement of κ. Finally, both the experimental and computational results suggest that decreasing the fraction of the θ phase in the eutectic compounds increases the overall κ of the Al–Cu connection, which can be exploited further for enhancing the overall thermal conductivity of cooling devices.

2. Materials and methods

2.1. Numerical techniques

In order to simulate the κ_l of the Al–Cu system, a $10 \times 10 \times 10$ face centered (fcc) single crystal Al cube (40.4 Å width) was constructed via Atomsk [25]. Next, Al atoms were randomly substituted with Cu atoms based on the desired atomic percentage of 5, 10, 15, 20, 25 and 30. The interatomic potential used in this study was obtained by a second nearest-neighbor modified embedded atoms method (2NN MEAM) that already showed its ability to predict different phases of the Al–Cu system and their properties with acceptable accuracy [26]. In addition, this type of interatomic potential has shown better accuracy for κ_l prediction [27]. To find out the preferred position of atoms, the systems were initially relaxed at 300 K for 20 ps via a Canonical (NVT) ensemble, then an isothermal–isobaric (NPT) ensemble for 20 ps. Subsequently, to imitate the effect of heat treatment at the temperature that the eutectic compounds form, a Monte Carlo algorithm was run for 200 ps. This algorithm switched the position of atoms to minimize the system's potential energy while the system evolved at 773 K (500 °C) under the NPT ensemble [28]. This method has already proven successful in predicting thermodynamically stable phases at desired temperatures for other materials [29]. Subsequently, the systems were cooled down to 300 K in 100 ps and were reproduced in the [001] direction to 2, 3, 4, 5, 6, 7, 8, 9, 10, 15, 20, and 25 times the original length of the system to incorporate the effect of system size on the thermal conductivity. The acquired systems were again relaxed via NVT and NPT ensembles before measuring the thermal conductivity. Notably, all MD simulations were performed utilizing the large-scale Atomic/Molecular Massively Parallel Simulator (LAMMPS, 23 June 2022 version) [30].

A reverse NEMD method proposed by Müller-Plathe and implemented in LAMMPS [20, 31] was utilized to calculate the thermal conductivity of the systems. In this method,

the systems were equilibrated in a microcanonical (NVE) ensemble for 100–250 ps and were divided into ten bins in the z direction. Every 50 fs, the kinetic energy of the five atoms with the lowest kinetic energy at the center bin was swapped with the five atoms possessing the highest kinetic energy in the bin at the end of the system. To increase the accuracy of the temperature sampling, overlapping bins half the size of previous bins were utilized. After the equilibration, the temperature gradient and the energy accumulation were measured for 100 ps, then converted to thermal conductivity.

Previous studies have shown a significant size effect on the predicted κ_{l}, which is due to the sample length being smaller than the bulk mean free path of phonons. More specifically, if a phonon is emitted from the hot reservoir of the sample (here the central bin) and the length it travels is smaller than its mean free path, it would pass through without scattering, which is also referred to as ballistic transportation. However, as the sample size is increased, the chance of phonon scattering will increase, thus transforming the ballistic to diffusive transport. This transformation is essential as the phonons of ballistic transport contribute less to the κ_{l}, which leads to an underestimation as compared to the bulk material $(\kappa_{\mathrm{l,\,bulk}})$ [32, 33]. The primary constraint in simulating the full mean free path of phonons is their large size, which demands extensive MD simulations. To solve this issue, Sellan *et al* [32] proposed an analytical solution establishing a relationship between the κ_{l} and the sample length L:

$$\kappa_{\mathrm{l}}(L) = \sum_{\nu}\sum_{K} c_{\mathrm{ph}} \upsilon_{\mathrm{g},z}^{2}(K,\nu)\,\tau_{\infty}(K,\nu) \times \left[1 + \frac{2\left|\upsilon_{\mathrm{g},\nu}(K,\nu)\right|\tau_{\infty}(K,\nu)}{L}\right]^{-1} \quad (2)$$

where c_{ph} is the volumetric specific heat of each mode, K is the wave vector, ν is the dispersion branch, and $\upsilon_{\mathrm{g}}(K,\nu)$ is the group velocity vector and τ is the relaxation time. It is possible to describe the above relationship via $\frac{1}{\kappa_{\mathrm{l}}} = \chi \times \frac{1}{L}$ in which χ is the unknown function describing the relationship. Therefore, it can be argued that as $\frac{1}{L} \to 0$, $L \to \infty$ and $\kappa_{\mathrm{l}} \to \kappa_{\infty}$, which is the bulk value $\kappa_{\mathrm{l,\,bulk}}$. Thus, using a Taylor-series expansion, this relationship can be approximated:

$$\frac{1}{\kappa_{\infty}} = \chi(0) = \chi\left(\frac{1}{L}\right) + \frac{\chi'\left(\frac{1}{L}\right)}{1!}\left[-\frac{1}{L}\right] + \frac{\chi''\left(\frac{1}{L}\right)}{2!}\left[-\frac{1}{L}\right]^{2} + \ldots. \quad (3)$$

Based on this approach, a method has been proposed to predict κ_{l} via truncating the terms after the first order, i.e. using a linear extrapolation to predict bulk thermal conductivity. A noticeable number of works have already used this method to simulate the κ_{l} [19, 34–38]. However, several studies pointed out possible issues with this method. One problem is that, as this method truncates some of the parameters of the relationship, it loses accuracy if the relationship between the κ_{l} and the sample length deviates from linearity [32, 39]. In addition, if the κ_{l} values collected for the linear extrapolation do not represent a sufficient length, it might misrepresent a non-linear behavior as linear. To solve this issue, ML methods were implemented in the current study as a replacement for linear extrapolation. Specifically, support vector machine with radial basis function (SVM-RBF) kernel, SVM with polynomial (SVM-POLY) kernel, and the random forest (RF) algorithm were trained utilizing the data acquired from the MD simulations. Subsequently, the accuracy of the models was evaluated via a test dataset[3] using the root mean squared error (RMSE). To increase the prediction power of the models, their hyperparameters were optimized utilizing the grid search method and bootstrapping.

[3] The datasets utilized in this study are provided in supplementary material table S1.

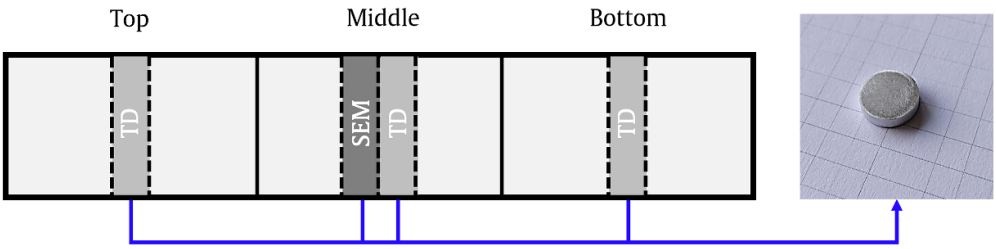

Figure 1. Positions of samples machined from the cast ingot for thermal conductivity (TD) and scanning electron microscopy (SEM) with an example of a machined sample shown in the photo on the right-hand side.

Table 1. Chemical compositions of cast samples and their measured densities.

Sample name	Al (at.%)	Cu (at.%)	Density (g cm^{-3}) at 25 °C
Al5Cu	95	5	2.91
Al10Cu	90	10	3.15
Al15Cu	85	15	3.38
Al20Cu	80	20	3.65
Al25Cu	75	25	3.89
Al30Cu	70	30	4.16

Finally, the best model was chosen to predict κ_{bulk} for each composition. All the ML methods were implemented in Python programming language using sci-kit learn libraries [40].

2.2. Experimental methods

In order to measure the thermal diffusivity of the eutectic Al–Cu samples, pellets of high-purity aluminum (Hydro Aluminium High Purity GmbH, Grevenbroich, Germany) with a purity of >99.87% and copper pieces of 99.65% purity (Hans-Erich Gemmel & Co. GmbH, Berlin, Germany) were weighted via a laboratory scale for each composition as shown in table 1. A vacuum induction melting device (MC50, Indutherm GmbH, Walzbachtal, Germany) was utilized to melt and mix the elements via inductive stirring for 5 min before casting them into a cylindrical cavity of a steel die. To increase the homogeneity of the ingots in terms of chemical composition and grain size of the samples, the ingots were homogenized inside a furnace at 500 °C for 48 h in air atmosphere. To incorporate the effect of gravity on the composition of the ingots, four cylindrical samples were sectioned from the top, middle, and bottom parts of the ingots as shown in figure 1. Subsequently, these samples were machined down to 10 mm diameter and 3 mm thickness. Their average densities were measured at room temperature (table 1) using the Archimedes principle via a density measurement scale (2200, MK Industrievertretungen, Germany).

To measure the thermal diffusivity of each composition, the sample surfaces were ground employing a 200-grit emery paper to remove the oxide layers, cleaned via ethanol, and spray-coated with a thin layer of graphite. This black graphite layer was applied to increase the energy absorption by the samples ensuring a homogeneous distribution of the energy in the samples. Subsequently, the xenon flash pulse method was used (Netzsch, LFA 447 NanoFlash), where an instantaneous pulse of energy is radiated to the sample, causing a temperature gradient detected

via an infrared camera to measure the thermal diffusivity [41, 42]. The thermal diffusivity value can be converted to thermal conductivity utilizing equation (4):

$$K = \alpha \times C_{\mathrm{p}} \times \rho \tag{4}$$

where α is the thermal diffusivity, C_{p} is the specific heat and ρ is the density. For each sample, five shots of the xenon flash were used to calibrate the device at room temperature, and then three shots were applied at higher temperatures of 50 °C, 100 °C, and 150 °C. The average diffusivities of these measurements are reported for each composition. For measuring the electrical conductivity of the samples, their surfaces were cleaned with ethanol and ten measurements were carried out on each sample by a portable eddy current device (SIGMATEST 2.069, Institut Dr Foerster GmbH & Co, Germany) at room temperature.

To investigate the chemical composition and surface morphology of the samples, following metallographic preparation of the samples, scanning electron microscopy (SEM, Zeiss Supra 55 VP) and energy dispersive x-ray (EDX) analysis (Bruker AXS GmbH, Karlsruhe, Germany) were carried out. For detecting grain boundaries and evaluating the grain size, electron backscatter diffraction (EBSD, Zeiss Auriga with Oxford detector) was utilized.

3. Results and discussion

Figure 2(a) presents results of the NEMD simulations of the κ_{l} for eutectic compositions of the Al–Cu compounds with various sample lengths. Accordingly, the κ_{l} of the compounds decreases notably with increasing Cu content, with a more pronounced change from 5 to 15 at.%. However, for the samples with a Cu content higher than 15 at.%, the decrease in κ_{l} is not substantial. When the change of the simulated $1/\kappa_{\mathrm{l}}$ with $1/L$ is compared for the six Al–Cu compounds (figure 2(b)), two regions with different slopes are prominent: one for the shorter and one for the longer samples. Implementing the conventional linear extrapolation method to predict the $\kappa_{\mathrm{l,\,bulk}}$ would result in an inaccurate prediction due to high fitting error, and thus a different approach should be taken. However before performing any fitting or prediction, it was necessary to ensure that the change in the slope was not an artifact of the simulations.

There are three possible reasons for the observed changes induced by varying the Cu content of the compounds (figure 2), and the first one might be associated with the divergent term of the κ_{l} as proposed by Hu *et al* [39]. In particular, for one-dimensional samples with small sizes, the divergent term of the κ_{l} is negligible. However, as the length of the samples increase, κ_{l} approaches infinite thermal conductivity, such that the intercept of the extrapolation on the $1/\kappa_{\mathrm{l}}$ would be negative. In contrast to one-dimensional samples, for nanowires, the long wavelength phonons result in higher scattering that prevents divergence in infinite length limit. Therefore, the values of κ_{l} converge to finite values [39], which is the case for all the present compositions. Thus, the change in the slope cannot be due to the divergent term of the κ_{l}.

The second possible reason could be the dependence of κ_{l} on temperature along the sample length, which was proposed by Talaat *et al* [38]. Specifically, in NEMD methods, materials with κ_{l} highly dependent on temperature, would possess different κ_{l} values along the length of a sample. This difference would increase as the length of the sample increases, resulting in a non-linear temperature gradient along the sample length. This non-linearity would cause longer samples to have higher κ_{l} as a simulation artifact [38]. However, in the present samples, the magnitude of the temperature gradient was linear even for the longest Al30Cu samples (figure 3), which corresponds to the composition with the highest change in the slope of the

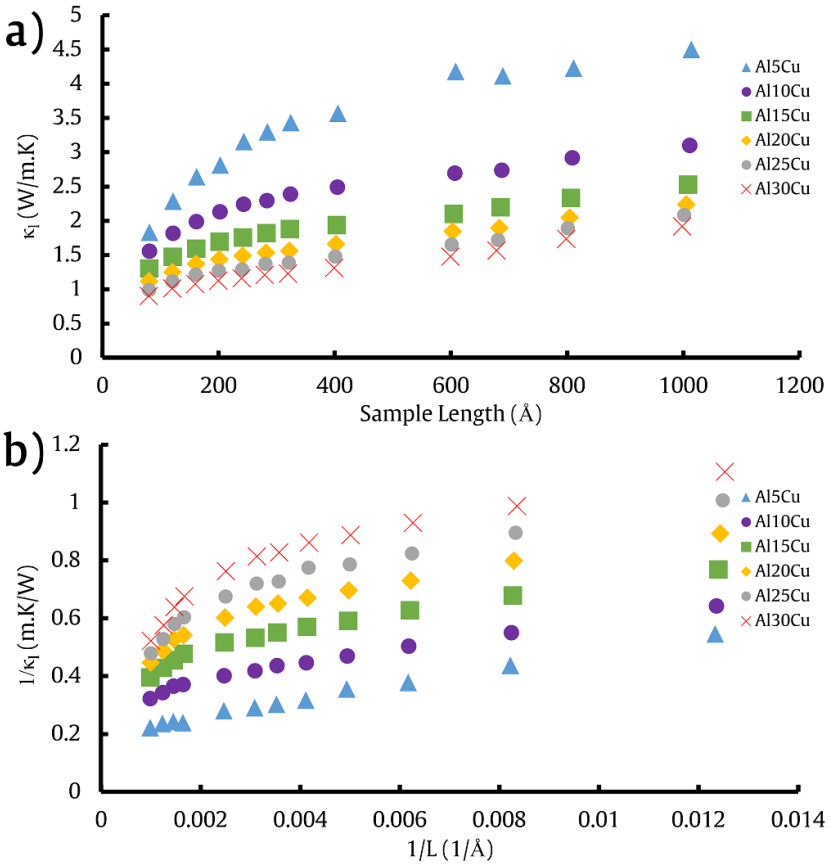

Figure 2. (a) κ_l values acquired from the NEMD simulations for different sample lengths, and (b) $1/\kappa_l$ values vs inversed length of the samples, highlighting the deviation from linear behavior.

simulated $1/\kappa_l$ with the $1/L$ curve (figure 2(b)). Thus, the effect of temperature dependence of κ_l can be ruled out as a potential reason for the observed changes in the current study.

The third possible reason is the incorporation of the contribution of phonons with a long mean free path to the κ_l value of the samples, which has been previously suggested as a reason for the increase in the κ_l values of the longer samples [19, 32, 37, 39]. As a result, one can deduce that the difference in the slope was not an artifact of simulation and the values of κ_l calculated via the NEMD method can be used for accurate prediction of the bulk κ_l in the Al–Cu eutectic system.

To extrapolate the simulated κ_l and predict the $\kappa_{l,\,bulk}$, three different ML methods, namely the SVM-RBF, SVM-POLY, and RF, were implemented on the dataset constructed with the MD simulation results. This dataset included the Cu at.% and $1/L$ as the input features, and the $1/\kappa_l$ as the output. In the first step, a grid search method was used to find the optimal hyperparameters for each of these methods[4]. In order to compare the performances of the models, a bootstrapping approach was used. This approach was utilized to establish the effect of the

[4] The optimal hyperparameters are provided in supplementary material table S2.

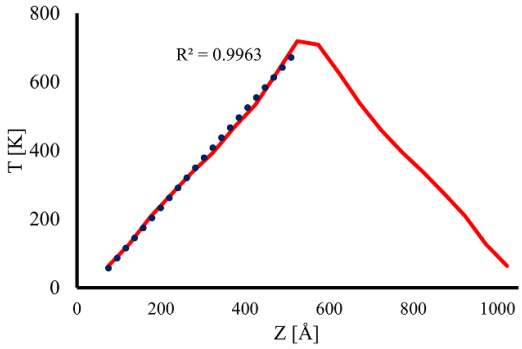

Figure 3. Temperature distribution within the longest Al30Cu sample; the magnitude of the measured thermal gradient exhibits linear behavior along the length of the sample.

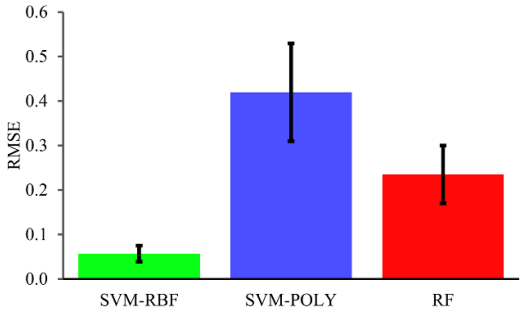

Figure 4. Comparison of the performance of three different ML methods employed, namely the SVM-RBF, SVM-POLY, and RF, based on bootstrap analysis.

training dataset on the performance of the models. Thus, the accuracy of the models can be assessed over different portions of the dataset, minimizing the bias caused by data sampling [43]. The three models were bootstrapped 100 times, and their RMSEs[5] were determined utilizing different test datasets. As a result, the SVM-RBF exhibited the lowest average RMSE of 0.056 with the least standard deviation of 0.018 (figure 4), and therefore, it was chosen for the prediction of κ_{l}.

Subsequently, the data were randomly separated into training and test datasets with a 20%–80% ratio to assess the ability of the SVM-RBF model to predict the unseen data. After training the model with the training dataset, both training and test datasets were predicted (cf. figure 5), and the SVM-RBF model could predict the unseen data of the test dataset with high accuracy, such that the RMSE was only 0.0121. This, indeed, demonstrates the ability of the SVM-RBF model to extrapolate and interpolate the values of $1/\kappa_{\mathrm{l}}$. Therefore, the SVM-RBF model was run on a synthetic dataset that incorporated $1/L$ values of 0 (for bulk samples) to 0.01 (10 Å), where $1/\kappa_{\mathrm{l}}$ was predicted for different compositions. The results presented in figure 6 demonstrate that the model could capture the behavior of the $1/\kappa_{\mathrm{l}}$ for both interpolation and extrapolation, which permits the use of the model to predict the $\kappa_{\mathrm{l,\,bulk}}$ from the intercept of

[5] Please refer to the supplementary material equation S1 for the mathematical definition of the RMSE.

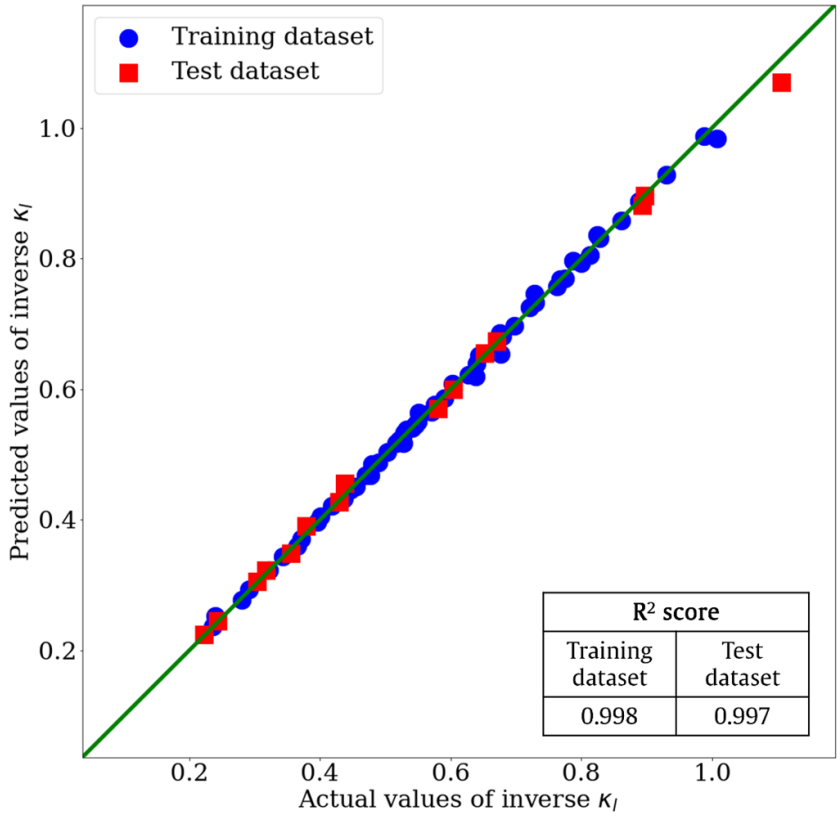

Figure 5. The performance diagram of the SVM-RBF model and the R^2 score values demonstrate the model's good fit and its predictive capability.

the predicted $1/\kappa_l$ with the y-axis. The values of the intercepts and their inverted values, i.e. $\kappa_{l,bulk}$, are tabulated in table 2 for each composition. The results presented herein are in good agreement with the values suggested by [10]. However, the present results also indicate the effect of Cu content on the κ_l, which follows the expected behavior of substitutional elements on the thermal conductivity [44, 45].

The actual chemical composition of the samples taken from the middle part of each ingot was measured utilizing EDX, and the measured values that are presented in table 3 are close to the intended compositions. Subsequently, the microstructures of the samples were investigated further utilizing backscattered electron microscopy (figure 7), revealing the change in the microstructure of samples with the increase in the Cu content. To be more specific, figure 7 shows that the point EDX measurements from the dark regions correspond to a composition of 98.5 at.% Al–1.5 at.% Cu, which is attributed to α-aluminum, while the bright areas represent a chemical composition of about 66.5 at.% Al–33.5 at.% Cu, which is attributed to the θ phase (Al_2Cu). Therefore, the Al30Cu sample contains mostly the θ phase, in addition to a small volume of α-Al, while the other compositions exhibit a rather mixed microstructure containing both α-Al and θ phases of different ratios. As a result of the difference in the amount of θ

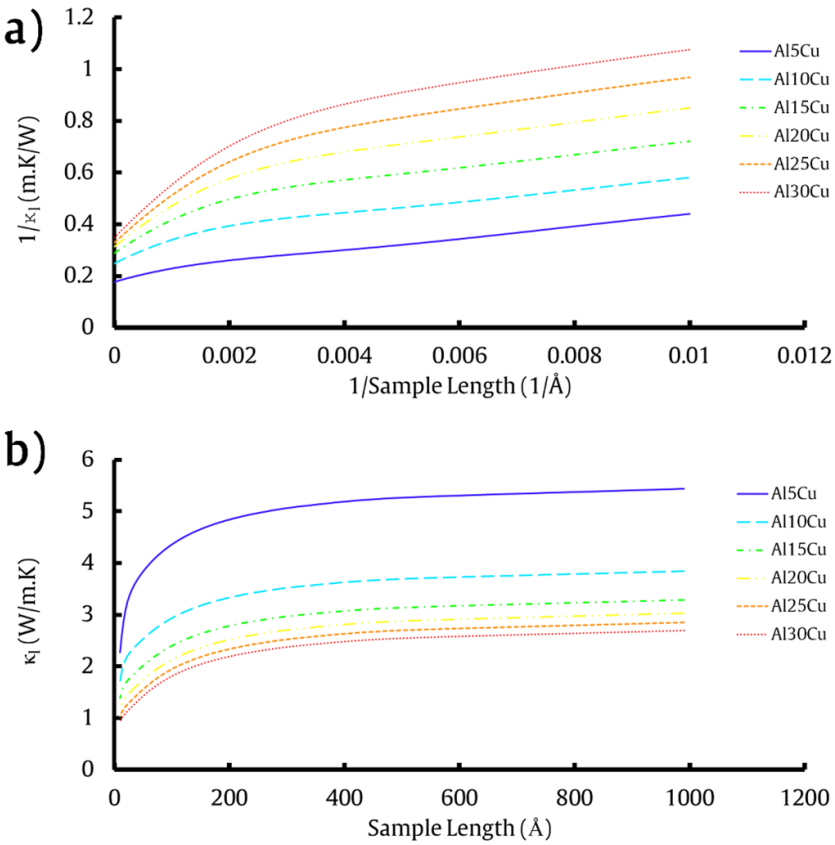

Figure 6. (a) The results of inverse κ_l predicted by the SVM-RBF model for Al–Cu samples with different inversed lengths, and (b) the corresponding actual κ_l values for different length of the samples.

Table 2. The values of the predicted y-axis intercepts for Al–Cu samples and the corresponding $\kappa_{l,\,bulk}$.

Sample	Intercept ($1/\kappa_l$)	$\kappa_{l,bulk}$(W (m·K)$^{-1}$)
Al5Cu	0.177	5.640
Al10Cu	0.249	4.016
Al15Cu	0.289	3.457
Al20Cu	0.312	3.205
Al25Cu	0.329	3.037
Al30Cu	0.349	2.866

phase, it is expected that the Al30Cu sample would have low thermal and electrical conductivity due to the fact that the θ phase has a higher amount of substitutional defects, promoting different scattering of phonons and electrons.

In addition to the chemical composition, grain boundaries also have a substantial effect on the thermal conductivity of materials [46]. Therefore, before cutting the cast ingots, they were heat treated in the furnace for 48 h at 500 °C for recrystallization and grain growth. To ensure

Table 3. Chemical compositions of the heat treated Al–Cu samples as measured by EDX.

Sample	Al (at.%)	Absolute error (%)	Cu (at.%)	Absolute error (%)
Al5Cu	95.77	2.5	4.23	0.3
Al10Cu	91.59	2.4	8.32	0.5
Al15Cu	86.71	2.3	13.07	0.7
Al20Cu	81.09	2.2	18.55	0.9
Al25Cu	75.50	2.0	23.98	1.1
Al30Cu	69.08	2.3	30.39	1.6

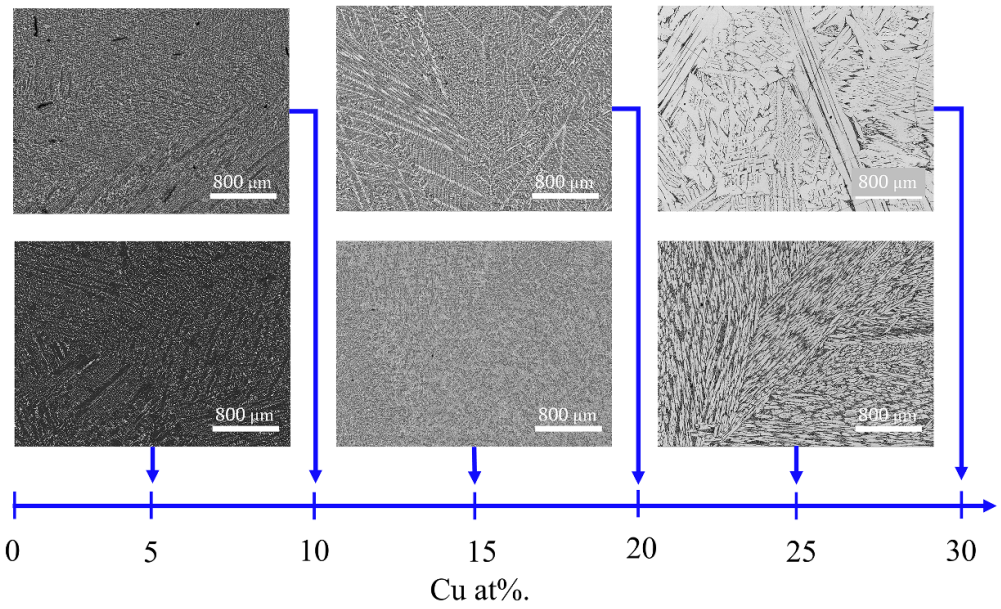

Figure 7. The microstructure of the Al–Cu samples following a heat treatment for 48 h at 500 °C.

the success of minimizing the grain boundaries, EBSD analysis was conducted on the samples prepared for SEM. Analyzing the EBSD images with the ImageJ software, it was deduced that each grain had an average area of 1 mm^2. Exemplary EBSD images of the surfaces of Al25Cu and Al30Cu are presented in figures 8 (a) and (b)[6]. The apparent grain sizes of the samples are larger than the ASTM G number of 0 [47], and thus, the grain boundaries are few enough to have a minimal effect on thermal conductivity.

The results of thermal diffusivity (α) measurements conducted with the xenon flash method at 25 °C and 100 °C are summarized in figure 9. The error bars shown in the figure include both the sampling position effect and α for several xenon shots, implying that varying the sample position causes statistically insignificant differences in thermal diffusivity.

A sharp decrease in α is noted when the Cu content increases from 0 at.% (i.e. pure Al) to 5 at.% (Al–5Cu), which is attributed to the introduction of both phonon and electron scattering

[6] EBSD images of other samples are provided in supplementary material figure S1 for the sake of brevity.

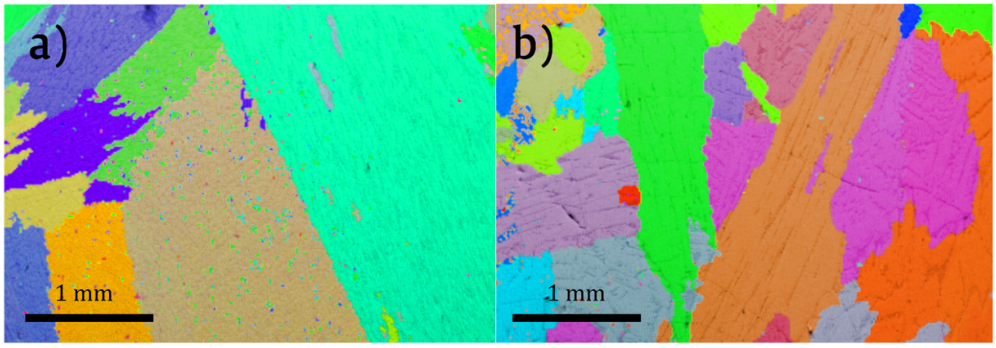

Figure 8. EBSD images of (a) Al25Cu and (b) Al30Cu samples following heat treatment at 500 °C for 48 h, demonstrating the presence of large grains in both compounds.

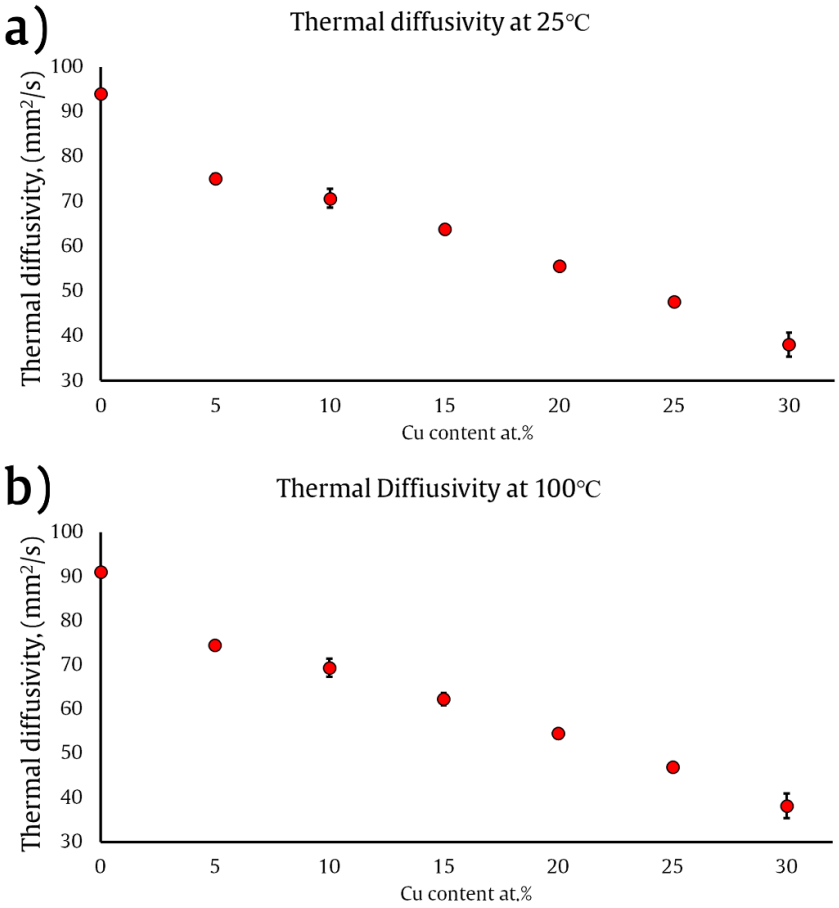

Figure 9. Thermal diffusivity of Al–Cu samples and pure aluminum (0 at.% Cu, used as reference material) at (a) 25 °C and (b) 100 °C.

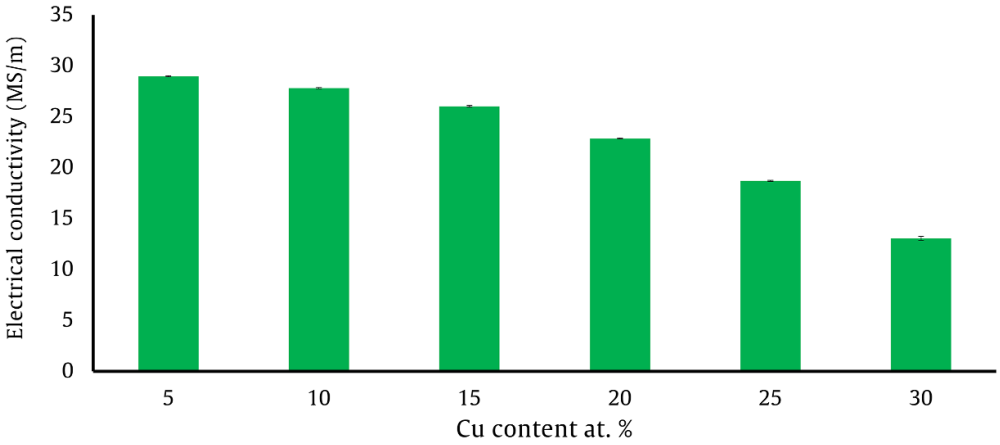

Figure 10. Electrical conductivity of post-heat treatment Al–Cu samples measured using the eddy current method; the error bars are hardly visible due to the negligible error of the measurements.

of Cu atoms as substitutional defects [48, 49]. For the remaining samples, α decreases almost linearly concomitant with increasing the Cu content. In addition, there is a minor temperature effect on α (roughly a 1% increase from 25 °C to 100 °C); however, such an increase can be ignored within the temperature range intended for cooling devices: although not shown herein for the sake of brevity, similar measurements at 50 °C and 150 °C support this argument. Using the experimentally determined thermal diffusivity values (calibrated by pure aluminum thermal diffusivity), the ρ from table 1, and the extrapolation of specific heat data acquired from the literature [50, 51], the experimental values of κ were calculated, and are presented in figure 11.

In order to evaluate the accuracy of the WFL equation for Al–Cu eutectics, it is necessary to measure the electrical conductivity of samples using a method that is not affected by contact resistance. Therefore, the σ of the samples were measured by the eddy current method and the results are presented in figure 10. Accordingly, the Cu addition significantly decreased the σ of the samples, reducing the σ to roughly half in the inspected range. Therefore, it is concluded that the increase in the θ phase, which results from increased Cu content as shown in figure 7, significantly decreases the σ. In addition, unlike the effect of increased Cu content on α, the values of σ do not decrease linearly, exhibiting a higher rate of decrease as the Cu content increases. Thus, the formation of the θ phase has a more pronounced effect on the σ as compared to α. This can be interpreted as κ_e being more affected by the θ phase formation than the overall κ. To calculate the κ_e, the σ values shown in figure 10 and the Lorenz value from the literature [52] were used in the WFL equation and the results are presented in figure 11.

A comparison of the κ_l calculated with MD simulations, the κ_e calculated using the WFL and the κ acquired via the xenon flash method (figure 11) revealed that the addition of κ_l to the κ_e enhances the accuracy of the WFL method with errors less than 10% for all compositions. If a measurement of the thermal conductivity via experimental methods is not possible, calculation of κ_l via MD simulations and calculation of κ_e via WFL equation can be a useful replacement. In addition, although the contribution of κ_e is the dominating factor of κ in Al–Cu system, in other systems with lower electronic and higher lattice contributions, κ_l calculated via MD simulations is indispensable for accurate prediction. The acquired results are also helpful in optimizing the parameters of the compound casting to enhance the overall κ of

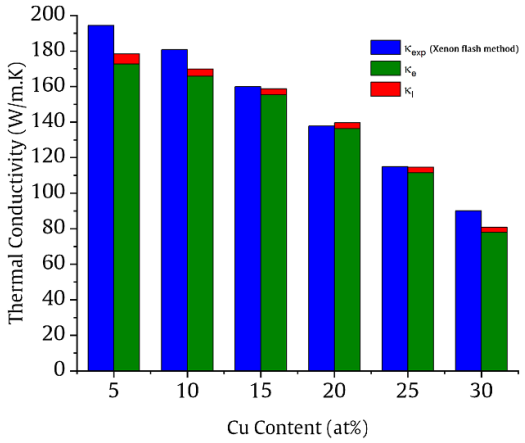

Figure 11. Comparison of the results acquired using the xenon flash method (κ_{exp}) and those obtained by the MD simulations (κ_{l}) and upon conversion of electrical conductivity utilizing the WFL (κ_{e}).

a cooling device. For instance, a previous study by Fromm *et al* showed that the connection made by compound casting under an XHV atmosphere mainly consists of a eutectic composition with about 17 at.% Cu and θ phase, followed by a small zone of Cu-rich intermetallics [8]. Based on both the experimental and the simulated results of this study, for an enhanced κ of an Al–Cu connection, increasing the portion of the Al-rich eutectic region would be beneficial. This is due to the fact that regions with compositions close to the θ phase (such as the Al30Cu sample) have roughly 50% less κ than the Al-rich ones. However, since in compound casting of Al–Cu, the connection relies on diffusion of elements, a short diffusion duration, resulting in a lower amount of Cu content, would cause a connection with insufficient mechanical properties. Considering the outcome of this study that suggests the minimization of the θ phase, and the fact that the elimination of the θ phase will deteriorate the mechanical properties of the Al–Cu bonds, superior Al–Cu connections could be achieved through the optimization of compound casting parameters to control the diffusion of Cu during the casting process.

4. Conclusions

In this study, the thermal conductivity (κ) of Al–Cu eutectic compositions was determined utilizing a combined computational and experimental approach with the aim of enhancing the overall κ of parts made with compound casting. In particular, using reverse NEMD, the lattice thermal conductivity (κ_{l}) of six Al–Cu eutectic compounds with 5–30 at.% Cu was simulated for various sample lengths. Subsequently, three ML models (SVM-RBF kernel, SVM-POLY kernel, and RF), were developed to predict the bulk κ_{l}. The performances of these models were compared using the bootstrap method, and the SVM-RBF kernel was found to have the best predicting capabilities. Employing this model, the bulk κ_{l} was predicted for the samples, with results showing that the addition of Cu has a significant effect on the κ_{l} of the Al–Cu compounds. In addition, these results remained in good agreement with those of the previous studies. To validate the computational approach and enhance the knowledge of the κ in Al–Cu eutectics, the samples were produced by the induction melting method and heat-treated for

48 h at 500 °C for recrystallization and growth. Three samples were machined from the heat-treated ingots' top, middle, and bottom parts to measure the thermal diffusivity for increased accuracy and carry out microstructural characterization. The experimental results showed a similar decrease in the κ due to an increased amount of Cu. In addition, it was demonstrated that utilizing the MD simulations to calculate κ_l can enhance the estimations made by WFL, presenting a new approach in cases where the measurement of κ via experimental methods is not possible. Moreover, the present results suggest the importance of elemental diffusion on κ, as the compounds with higher Cu content and θ phase can have less than 50% κ compared to the Al-rich eutectics. Overall, in addition to providing a novel approach to determine κ, the results of this study also warrant further investigation of the compound casting parameters influencing the diffusion in the Al–Cu connections.

Data availability statement

The data cannot be made publicly available upon publication because they are not available in a format that is sufficiently accessible or reusable by other researchers. The data that support the findings of this study are available upon reasonable request from the authors.

Acknowledgments

This study was funded by the Deutsche Forschungsgemeinschaft (DFG, German Research Foundation)—Project-ID 394563137—SFB 1368. D Canadinc acknowledges the financial support provided by the Alexander von Humboldt Foundation within the Humboldt Research Award program.

ORCID iDs

A Nazarahari https://orcid.org/0000-0002-8430-6941
A C Fromm https://orcid.org/0009-0008-7209-4436
H C Ozdemir https://orcid.org/0000-0001-6763-5770
H J Maier https://orcid.org/0000-0003-2119-824X
D Canadinc https://orcid.org/0000-0001-9961-7702

References

[1] Razeeb K M, Dalton E, Cross G L W and Robinson A J 2018 Present and future thermal interface materials for electronic devices *Int. Mater. Rev.* **63** 1–21
[2] Guan F, Jiang W M, Li G Y, Jiang H X, Zhu J W and Fan Z T 2019 Interfacial bonding mechanism and pouring temperature effect on Al/Cu bimetal prepared by a novel compound casting process *Mater. Res. Express* **6** 096529
[3] Zhang Y, Ma J, Wei N, Yang J and Pei Q-X 2021 Recent progress in the development of thermal interface materials: a review *Phys. Chem. Chem. Phys.* **23** 753–76
[4] Chung D D L 2022 Performance of thermal interface materials *Small* **18** 2200693
[5] Razeeb K M, Dalton E, Cross G L W and Robinson A J 2017 Present and future thermal interface materials for electronic devices *Int. Mater. Rev.* **63** 1–21
[6] Nolte N, Lukasczyk T and Mayer B 2022 Investigation of the microstructure and properties of aluminum–copper compounds fabricated by the high-pressure die casting process *Metals* **12** 1314

[7] Holländer U, Wulff D, Langohr A, Möhwald K and Maier H J 2020 Brazing in SiH_4-doped inert gases: a new approach to an environment friendly production process *Int. J. Precis. Eng. Manuf.* **7** 1059–71
[8] Fromm A C, Barienti K, Selmanovic A, Thurer S E, Nurnberger F, Maier H J and Klose C 2022 Oxygen-free compound casting of aluminum and copper in a silane-doped inert gas atmosphere: a new approach to increase thermal conductivity *Inter. Metalcast.* (https://doi.org/10.1007/s40962-022-00910-w)
[9] Raumel S, Barienti K, Luu H T, Merkert N, Dencker F, Nurnberger F, Maier H J and Wurz M C 2023 Characterization of the tribologically relevant cover layers formed on copper in oxygen and oxygen-free conditions *Friction* 1–17
[10] Ho C Y, Ackerman M W, Wu K Y, Oh S G and Havill T N 1978 Thermal conductivity of ten selected binary alloy systems *J. Phys. Chem. Ref. Data* **7** 959–1178
[11] Yao Y, Fry J, Fine M E and Keer L M 2013 The Wiedemann–Franz–Lorenz relation for lead-free solder and intermetallic materials *Acta Mater.* **61** 1525–36
[12] Macia E 2009 Thermal conductivity in complex metallic alloys: beyond Wiedemann-Franz law *Phys. Rev.* B **79** 245112
[13] Zheng X, Cahill D, Krasnochtchekov P, Averback R and Zhao J 2007 High-throughput thermal conductivity measurements of nickel solid solutions and the applicability of the Wiedemann–Franz law *Acta Mater.* **55** 5177–85
[14] Stojanovic N, Maithripala D H S, Berg J M and Holtz M 2010 Thermal conductivity in metallic nanostructures at high temperature: electrons, phonons, and the Wiedemann-Franz law *Phys. Rev.* B **82** 075418
[15] Maznev A A and Wright O B 2014 Demystifying umklapp vs normal scattering in lattice thermal conductivity *Am. J. Phys.* **82** 1062–6
[16] Kagaya H-M, Serita E-I, Sato M and Soma T 1996 Lattice dynamics and Debye temperature of Al-Cu, Al-Si and Al-Ge alloy systems *Solid State Commun.* **100** 727–30
[17] Turney J E, Landry E S, McGaughey A J H and Amon C H 2009 Predicting phonon properties and thermal conductivity from anharmonic lattice dynamics calculations and molecular dynamics simulations *Phys. Rev.* B **79** 064301
[18] Dongre B, Wang T and Madsen G K H 2017 Comparison of the Green–Kubo and homogeneous non-equilibrium molecular dynamics methods for calculating thermal conductivity *Modelling Simul. Mater. Sci. Eng.* **25** 054001
[19] Severin J and Jund P 2017 Thermal conductivity calculation in anisotropic crystals by molecular dynamics: application to alpha-Fe_2O_3 *J. Chem. Phys.* **146** 054505
[20] Müller-Plathe F 1997 A simple nonequilibrium molecular dynamics method for calculating the thermal conductivity *J. Chem. Phys.* **106** 6082–5
[21] Xu K, Fan Z, Zhang J, Wei N and Ala-Nissila T 2018 Thermal transport properties of single-layer black phosphorus from extensive molecular dynamics simulations *Modelling Simul. Mater. Sci. Eng.* **26** 085001
[22] Ouyang Y, Yu C, He J, Jiang P, Ren W and Chen J 2022 Accurate description of high-order phonon anharmonicity and lattice thermal conductivity from molecular dynamics simulations with machine learning potential *Phys. Rev.* B **105** 115202
[23] Ouyang Y, Yu C, Yan G and Chen J 2021 Machine learning approach for the prediction and optimization of thermal transport properties *Front. Phys.* **16** 43200
[24] Jin S, Zhang Z, Guo Y, Chen J, Nomura M and Volz S 2022 Optimization of interfacial thermal transport in Si/Ge heterostructure driven by machine learning *Int. J. Heat Mass Transfer* **182** 122014
[25] Hirel P 2015 Atomsk: a tool for manipulating and converting atomic data files *Comput. Phys. Commun.* **197** 212–9
[26] Mahata A, Mukhopadhyay T and Asle Zaeem M 2022 Modified embedded-atom method interatomic potentials for Al-Cu, Al-Fe and Al-Ni binary alloys: from room temperature to melting point *Comput. Mater. Sci.* **201** 110902
[27] Abs Da Cruz C, Termentzidis K, Chantrenne P and Kleber X 2011 Molecular dynamics simulations for the prediction of thermal conductivity of bulk silicon and silicon nanowires: influence of interatomic potentials and boundary conditions *J. Appl. Phys.* **110** 034309
[28] Sadigh B, Erhart P, Stukowski A, Caro A, Martinez E and Zepeda-Ruiz L 2012 Scalable parallel Monte Carlo algorithm for atomistic simulations of precipitation in alloys *Phys. Rev.* B **85** 184203

[29] Huang X S, Liu L H, Duan X B, Liao W B, Huang J J, Sun H B and Yu C Y 2021 Atomistic simulation of chemical short-range order in HfNbTaZr high entropy alloy based on a newly-developed interatomic potential *Mater. Des.* **202** 109560
[30] Thompson A P *et al* 2022 LAMMPS—a flexible simulation tool for particle-based materials modeling at the atomic, meso, and continuum scales *Comput. Phys. Commun.* **271** 108171
[31] Zhang M, Lussetti E, de Souza L E and Muller-Plathe F 2005 Thermal conductivities of molecular liquids by reverse nonequilibrium molecular dynamics *J. Phys. Chem.* B **109** 15060–7
[32] Sellan D P, Landry E S, Turney J E, McGaughey A J H and Amon C H 2010 Size effects in molecular dynamics thermal conductivity predictions *Phys. Rev.* B **81** 214305
[33] Bao H, Chen J, Gu X and Cao B 2018 A review of simulation methods in micro/nanoscale heat conduction *ES Energy Environ.* **1** 16–55
[34] Lee Y, Lee S and Hwang G S 2011 Effects of vacancy defects on thermal conductivity in crystalline silicon: a nonequilibrium molecular dynamics study *Phys. Rev.* B **83** 125202
[35] Li K, Cheng Y, Wang H, Guo Y, Zhang Z, Bescond M, Nomura M, Volz S, Zhang X and Xiong S 2022 Phonon resonant effect in silicon membranes with different crystallographic orientations *Int. J. Heat Mass Transfer* **183** 122144
[36] Zhou M, Liang T, Wu B, Liu J and Zhang P 2020 Phonon transport in antisite-substituted hexagonal boron nitride nanosheets: a molecular dynamics study *J. Appl. Phys.* **128** 234304
[37] Krishnamoorthy A, Rajak P, Norouzzadeh P, Singh D J, Kalia R K, Nakano A and Vashishta P 2019 Thermal conductivity of MoS_2 monolayers from molecular dynamics simulations *AIP Adv.* **9** 035042
[38] Talaat K, El-Genk M S and Cowen B 2020 Extrapolation of thermal conductivity in non-equilibrium molecular dynamics simulations to bulk scale *Int. Commun. Heat Mass Transfer* **118** 104880
[39] Hu L, Evans W J and Keblinski P 2011 One-dimensional phonon effects in direct molecular dynamics method for thermal conductivity determination *J. Appl. Phys.* **110** 113511
[40] Pedregosa F, Varoquaux G, Gramfort A, Michel V, Thirion B, Grisel O, Blondel M, Prettenhofer P, Weiss R and Dubourg V 2011 Scikit-learn: machine learning in Python *J. Mach. Learn. Res.* **12** 2825–30
[41] Parker W J, Jenkins R J, Butler C P and Abbott G L 2004 Flash method of determining thermal diffusivity, heat capacity, and thermal conductivity *J. Appl. Phys.* **32** 1679
[42] Cowan R D 2004 Pulse method of measuring thermal diffusivity at high temperatures *J. Appl. Phys.* **34** 926
[43] Kulesa A, Krzywinski M, Blainey P and Altman N 2015 Sampling distributions and the bootstrap *Nat. Methods* **12** 477–8
[44] Zhao M, Pan W, Wan C, Qu Z, Li Z and Yang J 2017 Defect engineering in development of low thermal conductivity materials: a review *J. Eur. Ceram. Soc.* **37** 1–13
[45] Shen J, Zhang X, Chen Z, Lin S, Li J, Li W, Li S, Chen Y and Pei Y 2017 Substitutional defects enhancing thermoelectric $CuGaTe_2$ *J. Mater. Chem.* A **5** 5314–20
[46] Sood A *et al* 2018 Direct visualization of thermal conductivity suppression due to enhanced phonon scattering near individual grain boundaries *Nano Lett.* **18** 3466–72
[47] International A 2015 *ASTM E112-13 Standard Test Methods for Determining Average Grain Size* (West Conshohocken, PA: ASTM International) pp 19428–2959
[48] Edwards S F 1958 A new method for the evaluation of electric conductivity in metals *Philos. Mag. Lett.* **3** 1020–31
[49] Callaway J and von Baeyer H C 1960 Effect of point imperfections on lattice thermal conductivity *Phys. Rev.* **120** 1149–54
[50] Song Z-X, Li Y-D, Liu W-J, Yang H-K, Cao Y-J and Bi G-L 2021 Effect of La and Sc co-addition on the mechanical properties and thermal conductivity of As-cast Al-4.8% Cu alloys *Metals* **11** 1866
[51] Wei G, Huang P, Xu C, Liu D, Ju X, Du X, Xing L and Yang Y 2016 Thermophysical property measurements and thermal energy storage capacity analysis of aluminum alloys *Sol. Energy* **137** 66–72
[52] Hust J G and Sparks L L 1973 *Lorenz Ratios of Technically Important Metals and Alloys* (*Technical Note 634*) (National Bureau of Standards)